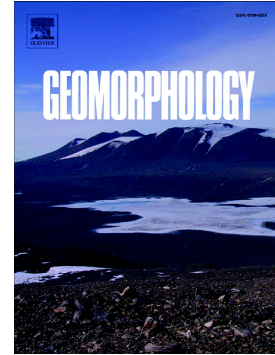# Accepted Manuscript

Simulating bank erosion over an extended natural sinuous river reach using a universal slope stability algorithm coupled with a morphodynamic model

Yannick Y. Rousseau, Marco J. Van de Wiel, Pascale M. Biron

Please cite this article as: Yannick Y. Rousseau, Marco J. Van de Wiel, Pascale M. Biron , Simulating bank erosion over an extended natural sinuous river reach using a universal slope stability algorithm coupled with a morphodynamic model, *Geomorphology* (2017), doi: 10.1016/j.geomorph.2017.08.008

Simulating bank erosion over an extended natural sinuous river reach using a universal slope stability algorithm coupled with a morphodynamic model

Yannick Y. Rousseau [a,*], Marco J. Van de Wiel [b], Pascale M. Biron [a]

[a] *Department of Geography, Planning and Environment, Concordia University, Henry F. Hall Building, Room S-H 1263, 1455 de Maisonneuve Blvd. W., Montréal, Canada, H3G 1M8. E-mail addresses: yanrousseau@gmail.com and pascale.biron@concordia.ca.*

[b] *Centre for Agroecology, Water and Resilience, Coventry University, James Starley Building, Room B02B, Priory Street, Coventry, United Kingdom, CV1 5FB. E-mail address: marco.vandewiel@coventry.ac.uk.*

Abstract

Meandering river channels are often associated with cohesive banks. Yet only a few river modelling packages include geotechnical and plant effects. Existing packages are solely compatible with single-threaded channels, require a specific mesh structure, derive lateral migration rates from hydraulic properties, determine stability based on friction angle, rely on nonphysical assumptions to describe cutoffs, or exclude floodplain processes and vegetation. In this paper, we evaluate the accuracy of a new geotechnical module that was developed and coupled with Telemac-Mascaret to address these limitations. Innovatively, the newly developed module relies on a fully configurable, universal genetic algorithm with tournament selection that permits it (1) to assess geotechnical stability along potentially unstable slope profiles intersecting liquid-solid boundaries, and (2) to predict the shape and extent of slump blocks while considering mechanical plant effects, bank hydrology, and the hydrostatic pressure caused by flow. The profiles of unstable banks are altered while ensuring mass conservation. Importantly, the new stability module is independent of mesh structure and can operate efficiently along multithreaded channels, cutoffs, and islands. Data collected along a 1.5-km-long reach of the semialluvial Medway Creek, Canada, over a period of 3.5 years are used to evaluate the capacity of the coupled model to accurately predict bank retreat in meandering river channels and to evaluate the extent to which the new model can

2

be applied to a natural river reach located in a complex environment. Our results indicate that key geotechnical parameters can indeed be adjusted to fit observations, even with a minimal calibration effort, and that the model correctly identifies the location of the most severely eroded bank regions. The combined use of genetic and spatial analysis algorithms, in particular for the evaluation of geotechnical stability independently of the hydrodynamic mesh, permits the consideration of biophysical conditions for an extended river reach with complex bank geometries, with only a minor increase in run time. Further improvements with respect to plant representation could assist scientists in better understanding channel-floodplain interactions and in evaluating channel designs in river management projects.

＊Corresponding author: E-mail address: yanrousseau@gmail.com.

1. Introduction

Morphodynamic models have been employed for decades by researchers and practitioners to examine the evolution of alluvial river channels (e.g., Rinaldi et al., 2008; Tal and Paola, 2010; Ham and Church, 2012). In particular, two-dimensional nonlinear and linear models based on the shallow water equations, combined with a computational mesh that can evolve because of sediment transport, are increasingly used to determine the morphological evolution of meandering channels (Darby et al., 2002; Langendoen et al., 2016). Most of these models involve a large number of assumptions and simplifications to combine fluvial and bank erosion processes into a runnable solution, often neglecting floodplain heterogeneity in terms of morphology (Pittaluga and Seminara, 2011), channel bedforms (Shen, 1984; Parker et al., 2011), multithreading (Camporeale et al., 2013), sedimentology and stratigraphy (Simon et al., 2000; Malkinson and Wittenberg, 2007; Lai et al., 2012), bank hydrology (Pollen, 2007; Pollen-Bankhead and Simon, 2010), and flow regimes. As a result, the contribution of these processes to channel evolution is poorly understood (Güneralp and Marston, 2012). In addition, riparian plants that alter channel/floodplain roughness and provide mechanical soil reinforcement (Abernethy and Rutherfurd, 1998; Van de Wiel and Darby, 2007; Thomas and Pollen-Bankhead, 2010) should be included in morphodynamic models, although this is seldom the case (Bertoldi et al., 2014). Finally, opportunities to establish spatial connections between floodplain components, for instance between hydrological processes and riparian plants (Perucca et al., 2007; Mitsch and Gosselink, 2010), are often missed (Malkinson and Wittenberg, 2007; Lai et al., 2012).

A few river models have been enhanced to include bank retreat algorithms (e.g., El Kadi Abderrezzak et al., 2016). The linear near-bank excess velocity approach (known as HIPS, from Hasegawa (1977) and Ikeda et al. (1981)) relies on an erodibility coefficient to lump the effects of flow, soil, and vegetation properties to bank retreat rates (see Johannesson and Parker, 1989; Zolezzi and Seminara, 2001; Posner and Duan, 2012), thus making it impossible to isolate the specific causes for retreat, and to *entirely* simulate long-term planimetric and morphological evolution owing to the lack of

analytical solution of neck/chute cutoff (Chen and Tang, 2012). In addition, these models do not guarantee sediment continuity and assume a flat-bedded channel with few perturbations (Coulthard and Van de Wiel, 2006; Pittaluga and Seminara, 2011). When riparian vegetation is considered, its effect is typically limited to altering bed roughness, although a few notable exceptions exist where vegetation was connected to other floodplain processes (e.g., Collins et al., 2004; Perucca et al., 2007; Iwasaki et al., 2016). Models based on HIPS concepts do, however, have the advantage of allowing for long reaches to be simulated at relatively low computational cost (e.g., Schwenk et al., 2015). A few non-linear morphodynamic models have also been coupled to physically based bank erosion modules (e.g., Darby et al., 2002; Lai et al., 2012; Langendoen et al., 2016). However, several limitations remain regarding these solutions. The most severe ones are probably their incompatibility with long spatiotemporal scales (Pittaluga and Seminara, 2011), the lack of physically based equations in the implemented bank stability assessment and retreat processes, and the integration of assumptions such as arbitrary bank and planform geometries (e.g., Duan and Julien, 2010; Langendoen et al., 2016). The main difficulty seems associated with the inclusion of processes acting at different spatiotemporal scales compared to the shallow-water flow equations employed in the hydrodynamic models (Williams et al., 2016a).

The integration of geotechnical algorithms applicable over long river reaches in a natural environment with complex floodplain has seldom been attempted (Rousseau et al., 2014a,b; Evangelista et al., 2015). This paper presents a novel set of algorithms implemented in a new physics-based, deterministic model of channel-floodplain coevolution. The model is capable of simulating mass wasting events, including river bank failures, while also taking into account the specific biophysical context. Here, it is integrated into a two-dimensional unstructured grid morphodynamic model (Telemac-Mascaret), but it could also be implemented in other modelling software with relatively minor adjustments. The novel aspects included in the present modelling investigation is fivefold: (i) physics-based algorithms allowing us to parameterize lateral erosion using physical, measurable quantities; (ii) a genetic algorithm that can

automatically select between rotational and translational failure mechanisms, depending on local biophysical conditions; and allow (iii) larger spatial and temporal scales than commonly employed in physics-based bank erosion modelling because of greater computational efficiency; (iv) a bank erosion module independent of mesh structure, i.e., imposing a body-fitted coordinate system is not needed; and (v) model calibration using data from a complex natural site. Furthermore, because the model includes the interaction between an alluvial river channel and its (vegetated or nonvegetated) floodplain, it is able to simulate lateral river channel adjustments that can lead to the development of meandering, wandering, or braided river planform geometries. This paper thus directly addresses the issues identified by Williams et al. (2016b, p.6639) who noted that 'Future model development efforts should be directed toward improving the realism of bank erosion processes in the model. In particular, the bank erosion scheme needs to be made independent of grid resolution and orientation.'

2. Overview of model components

The geotechnical and riparian vegetation modules presented here were integrated into the Open Telemac-Mascaret suite of mathematical solvers to include additional fluvial processes, namely lateral adjustments through mass wasting of river banks and the effects of floodplain vegetation on geotechnical stability (Rousseau et al., 2014a, b).

2.1. Hydrodynamics

The two-dimensional (2D) version of Telemac was selected to minimize computation time, although the three-dimensional (3D) version could easily be coupled to the new modules if required in future projects. The equations governing fluid motion, in their nonconservative form and Cartesian coordinates, are described in Galland et al. (1991). The Smagorinsky (1963) model was selected to consider turbulent viscosity whilst minimizing computational effort. The default advection scheme, i.e., the method of characteristics, was selected for horizontal flow velocities and depth. For boundary conditions, flow discharge and uniform velocities were imposed at the channel inlet with a free surface elevation at the

outlet. In all simulations, the inlet of the flow comprised the wet nodes on the left domain side, whereas the outlet included all the mesh nodes located on the right domain side so that the outlet may adjust its location during a simulation.

2.2. Sediment transport and bed deformation

Sediment transport is calculated by the module Sisyphe. The Meyer-Peter and Müeller (1948) bedload formula was selected to calculate transport rates during simulations because of its compatibility with respect to sediment grain size at our field site (see below). Hiding/exposure is calculated using Egiazaroff (1965). The formulae related to the configurations considered in this study are thoroughly described in Villaret (2010). Bed evolution owing to bedload transport is calculated using the Exner equation.

The sediment transport module Sisyphe includes an algorithm that can simulate sediment slide; this was deactivated to let geotechnically stable river banks be steeper than the friction angle of sediment and, more importantly, to prevent having two modules competing for a single process. An option was enabled to include curvature effects on the direction of particle entrainment to compensate for the fact that the flow is depth-averaged. This feature was enabled in all simulations because of its relevance for the study of meandering processes. The effects of transport magnitude and direction on local topography are estimated using Koch and Flokstra (1981).

2.3. Lateral adjustments

The primary objective of this research was to develop an alternative methodology to simulate river bank retreat within a computational fluid dynamics (CFD) model, using a set of algorithms that is compatible with unstructured meshes, for a wide spectrum of alluvial rivers and with any modelling code offering finite element spatial discretization. This new framework relies almost completely on vector-based spatial analysis. In the generic framework, the stability submodel ignores the location of channel boundaries. Instead, it performs stability assessments across the floodplain, considering flow conditions, antecedent soil moisture, soil and sedimentological properties, and plant cover (if the vegetation module is enabled, see below). The channel planform will evolve when the banks are unstable along its boundaries.

The module is divided into five components. A landscape analysis algorithm generates a network of transects along which slope stability assessments are performed during a morphodynamic simulation (see the inset in Fig. 1). Although this algorithm can be configured to detect potentially unstable slopes anywhere across the simulation domain, for the current study an option was enabled to perform the analysis strictly along the external river bank of meander bends through edge detection. A genetic algorithm searches for the geometry of the most likely failure profile and returns the lowest safety factor (F_s, the ratio of shear strength to shear stress – see Eqs. 3-4 below) encountered. The geotechnical module
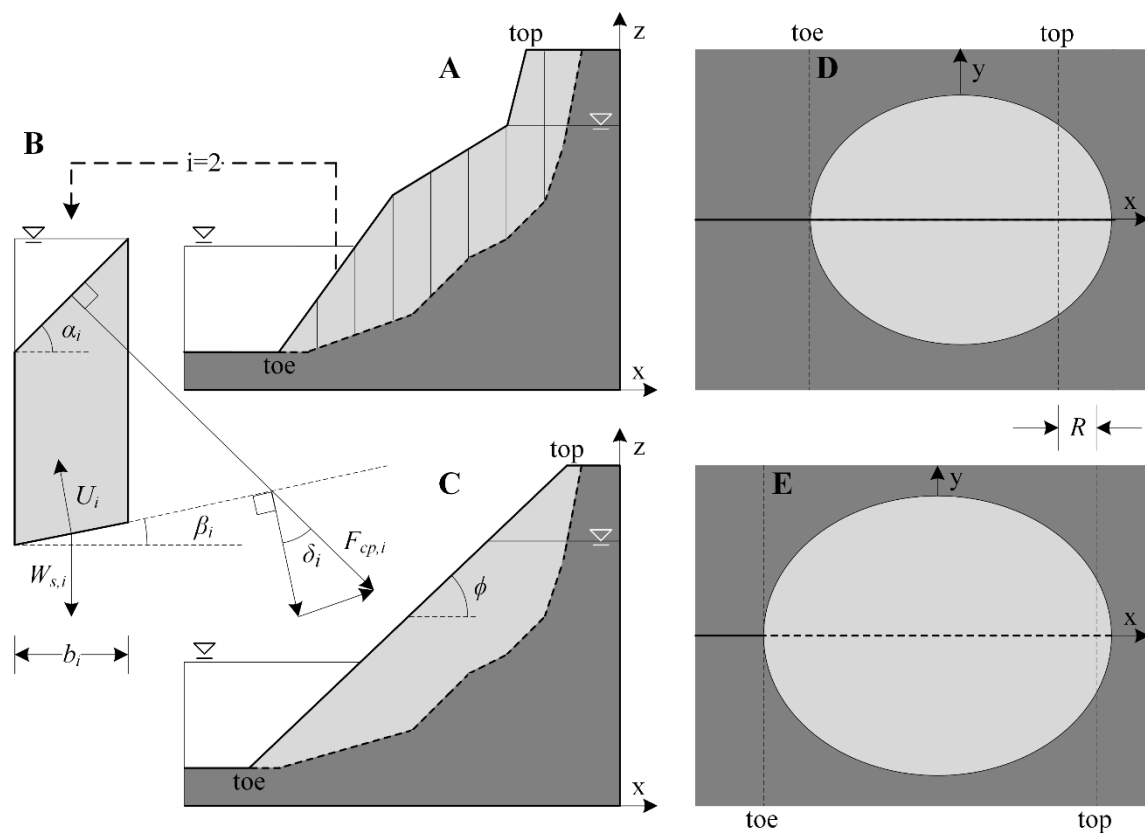
Fig. 1. Bank slope stability assessment using Bishop's simplified method of slices. (A) Initial profile, indicating stable bank region (dark gray) and failure block (light gray). (B) Stability is calculated based on forces acting on vertical slices through the failure block (Eqs. 3-4). (C) Profile following deposition of the failure block at the friction angle of the bank material. Note that this is a 2D transect of a 3D bank; the volume of the failure block in C is the same as in A. The upper limit of the failure block in C, i.e., a planar 3D surface within an elliptical zone, is adjusted to ensure that the two failure block volumes are equal. Elliptical zones affected by (D) block failure and (E) deposition. The character R indicates the distance of bank retreat.

includes a river bank hydrology module that computes water table elevation in the river bank as a function of flow stage and hydraulic conductivity. Finally, the algorithm analyses the geotechnical stability of a river bank in search of a failure block geometry that minimizes the safety factor (during the erosion phase, the unknown is the lower extent of the failure block, represented by the dashed line in Fig. 1A), removes the unstable failure block and deposits the material downslope at the friction angle (Fig. 1C, also see section 2.3.5 below), and updates the computational mesh nodes while ensuring mass conservation (the unknown is the upper extent of the altered unstable block during the deposition phase) (see Rousseau et al. (2014a,b) for more details). The upper extent of the post-failure block is a 3D planar surface with an elliptical shape. The mesh nodes affected by a failure are those located in the elliptical erosion and deposition zones (Figs. 1D and 1E) with the vertical displacement at a node inversely proportional to its horizontal distance on the stability-analysis transect.

2.3.1. Terrain analysis

The geotechnical model evaluates terrain stability along a large number of analysis transects carefully placed across the landscape. Each transect is oriented in the direction of the steepest ascent and adjusted in length to extend from the lowest to the highest elevation in this direction. Transect orientation is done by spinning a transect of length *trLen* around its center of mass and selecting the angle that minimizes the surface elevation's root mean square error between the points comprised in two transects located on each side of a trial transect at a distance *trLen* / 2. A smoothening stage adjusts the direction of each transect with respect to the direction of their immediate neighbours. Each transect is extended until an increase in length no longer leads to any substantial elevation change, defined by a threshold parameter (10° in our simulations) to improve efficiency, as otherwise geotechnical stability would be evaluated for very shallow banks that are unlikely to erode. Each transect is then transposed into a 2D bank profile, which is analysed for stability using the method of slices and powered by a genetic algorithm, both of which are described in detail in the following sections. By default, transects regenerate at each iteration of the geotechnical module. However, regeneration was disabled in our simulations to facilitate the statistical

comparison of retreat rates between scenarios. This strategy could be adopted because of the relatively low retreat rates and short simulations in our study. Although the location of transect centers was constant in time, each transect elongated and rotated to adjust to the evolving bank morphology.

Several options are available in the geotechnical module to define transect density, distribution pattern, and admissibility criteria, e.g., in terms of wetness/dryness and length. In the context of a study involving lateral erosion in meandering channels, the edge detection algorithm was selected; it distributes transects at equal distance along solid-liquid boundaries. Its independence of mesh structure means that it can efficiently detect river banks along multithreaded channels, cutoffs, and islands.

2.3.2. Genetic algorithm

Any slope stability analysis includes an algorithm that devises a set of potential slip surfaces to be evaluated for their geotechnical stability. Given a 2D geotechnical stability analysis, a solution with identifier *id* is a series of connected nodes delineating the lower limit of an unstable soil block, i.e., the dashed line in Fig. 1A. Therefore, a solution can be described by the following vector:

$$\vec{S}_{id} = \{\vec{v}_1, \vec{v}_2, ..., \vec{v}_{n-1}, \vec{v}_n\} \tag{1}$$

where $\vec{v}_i$ is the node at rank *i* along a slip surface. The solution with the lowest F_s value is the most likely to occur.

Grid-search patterns are usually employed to list potential slip surfaces. For instance, this can be achieved by varying the location of the centre of the arc describing the shape of a circular slip surface, along with its radius. Here, a genetic algorithm with tournament selection, improved from the work of Li et al. (2010), was implemented in the geotechnical module to converge toward a critical solution more rapidly. A *child* solution is created by combining two existing solutions, *i* and *j*, such that

$$\vec{S}_{child} = \eta \vec{S}_i + (\eta - 1)\vec{S}_j \tag{2}$$

where $\eta = [0,1]$ is a randomly generated crossover ratio. During crossover, mutation has a probability of happening, in which case a randomly selected node comprised in *child* solution is displaced. A set of

matching rules, namely partner exclusivity, child count policy, and prevention of breeding between relatives, allows the variability within the pool of solutions to be optimized (Li et al., 2010). For example, a child count policy means that two solutions S_i and S_j (a solution is a potential slip surface or the dashed line in Fig. 1B) can produce a predefined maximum number of solutions after randomly mixing their geometrical characteristics. The lack of such a policy limits genetic variability and thus increases the time required to converge toward a stable solution, i.e., finding the failure block associated with the lowest safety factor. Finally, a user-specified migration rate dictates the probability for a solution to be created randomly rather than being the result of a crossover.

In the current context, we can define a generation as the set of n solutions that were created from an initial population. After each generation, the most critical slip surface(s) are kept, the least critical are discarded, and new randomly selected surfaces survive to the next round. The search process terminates when the most critical slip surface remains unaltered for a number of consecutive generations.

2.3.3. Slope stability assessment

Bishop's (1955) modified method of slices (Fig. 1) was slightly adjusted to quantify the geotechnical stability of the soil along a transect while considering the flow's confining pressure and soil pore-water pressure. Combined with the genetic algorithm, it can produce planar, circular, and noncircular slip surfaces. Given a 2D bank profile and potential slip surface, the following set of equations must be solved by iteration:

$$F_s = \frac{\sum_{i=1}^{n} \dfrac{cb_i + \left(\gamma_{s,i} + F_{cp,i} - U_i b_i\right)\tan\phi}{m_i}}{\sum_{i=1}^{n} \gamma_{s,i}\sin\beta_i + F_{cp,i}\sin\delta_i} \tag{3}$$

$$m_i = \cos\beta_i + \frac{\sin\beta_i \cdot \tan\phi}{F_s} \tag{4}$$

where F_s = safety factor; $\gamma_{s,i}$ = weight of soil material in slice i out of n; U_i = the pore water pressure at the base of a slice of width b_i, basal angle β_i, and top angle α_i; δ_i = angle between the result of hydrostatic

confining force and normal to failure plane; ϕ = friction angle of the soil material; and m_i = m-term in Bishop formula. Pore-water pressure is given by

$$U = \frac{\rho g}{z_{wt} - z_b} \tag{5}$$

where g = acceleration owing to gravity, z_{wt} = elevation of the water table, and z_b = elevation at the base of a slice. A first approximation of F_s value is done using the ordinary method of slices (Fellenius, 1927). The confined water pressure is given by

$$F_{cp,i} = \gamma_{w,i} \cos \beta_i \tag{6}$$

where $\gamma_{w,i}$ = weight of water. Any solution resulting in a safety factor lower than unity is said to be unstable and is expected to result in a slope failure.

2.3.4. River bank hydrology

A saturated river bank, combined with a falling flow stage, can trigger mass wasting events (Thorne, 1982). To account for the lag effect between free surface and water table elevations, a simple river bank hydrology module is used to calculate water table elevation. According to this module, water table elevation (z'_{wt}) at a time $t = t_0 + \Delta t$ is given by

$$z_{wt}' = z_{fs} - \left(z_{fs} - z_{wt}\right)e^{-k\Delta_t} \tag{7}$$

where t_0 = time at the previous iteration, Δt = time step, $t = t_0 + \Delta t$ = time at the current iteration, z_{wt} = water table elevation at time t_0, z'_{wt} = water table elevation at time t, z_{fs} = flow surface elevation at time t_0, and k = rate of convergence of the water table elevation toward z_{fs}. The constant k is adjusted according to the hydraulic conductivity of the bank material and thus represents how quickly the water table adapts to a change in the river's flow stage. Two k-values are required per simulation: one for the rising limb of a flood hydrograph, and one for its falling limb (see values below).

2.3.5. Slump block removal and deposition

The slope stability analysis performed along each transect returns the side profile, i.e. the 2D curve representing the critical slip surface (Fig. 1A). Each mesh node affected by mass wasting relocates according to its position (d_B/r_B, d_A/r_A) with respect to the boundaries of an elliptical erosion surface (Fig. 2). The ellipse has the length of the unstable section of the analysis transect and a user-defined relative width, i.e., r_B/r_A in Fig. 2; a value of 0.75 was selected for our simulations to cover the bank region located between a transect's immediate neighbours. A mesh node located along the edge of the ellipse is not affected by a failure. Conversely, displacement computed is greatest along the transect for each d_A/r_A value. A mesh node located within the ellipse has a vertical displacement (dz) that is computed as a linear function of the distance between the transect and the edge of the ellipse, in the direction orthogonal to the transect, i.e.,

$$dz = dz_A \cdot \frac{d_B}{r_B \sqrt{1 - \left(\dfrac{d_A}{r_A}\right)^2}} \tag{8}$$

where r_A and $r_B = r_A \cdot k_f$ = lengths of the semiaxes A and B, k_f = width-to-length ratio of all ellipses defining an erosion or deposition zone, d_A and d_B = distances from the ellipse's centre to the mesh node along each semiaxis, dz_A = elevation change at a distance d_A from the centre of the ellipse in the direction of the mesh node x along the axis A. The value of dz_A is obtained by interpolating elevation change at node x_m using the two nearest transect nodes. Mesh elements that are intersecting the transect snap to the slip surface (lower line in Fig. 1A) after a vertical translation and/or a rotation around an axis orthogonal to the 2D profile. The volume of the unstable block is calculated by subtracting the pre- and post-failure computational meshes, assuming that the neighbouring transects are stable. The unstable slope material deposits in an elliptical zone at the toe of the slope at the friction angle of the bank material. An algorithm similar to the erosion algorithm is used, with one important distinction: a solver is required to ensure that the volume of eroded soil is equal to the deposited volume and thus guarantees mass conservation. Note that the elliptical zone where deposition occurs is usually not identical to the

ellipse in which erosion occurs as material moves downslope during a failure.

2.3.6. Soil properties

In its simplest configuration mode, the geotechnical module defines bank material in terms of soil class and degree of compaction. The other relevant sedimentological parameters, i.e., mean grain size, mass density, friction angle, cohesion, and porosity, are calculated using tabular data available in NAVFAC (1986), Swiss Standard SN 670 010b (1999), and MnDOT (2015). Soil material below the water table is assumed to be saturated; it is partially saturated if fine-textured and located above the water table while being affected by capillary rise; and it is dry otherwise. Default values can be overridden by the model user. Although the module is capable of recognizing multiple soil layers, bank material was assumed to have uniform properties in our simulations.
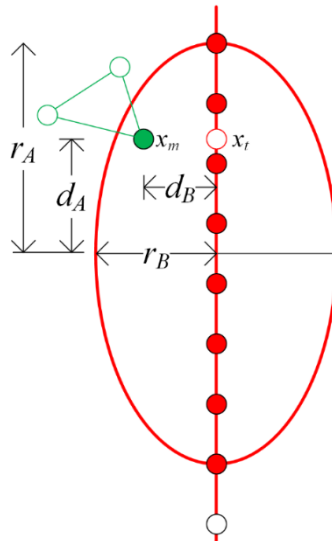
Fig. 2. Geometry of an erosion or deposition zone (Figs. 1D and 1E) within an elliptical zone with flatness r_B / r_A. Any mesh node x_m, located within the ellipse, as well as the red-filled nodes along the analysis transect are unstable. In erosion mode, the elevation change at mesh node x_m depends on the distance d_B. However, in deposition mode, the elevation of transect node x_t is assigned to mesh node x_m for each tridimensional planar surface representing a potential depositional fan surface.

2.3.7. Riparian vegetation

At each geotechnical iteration, the plant evolution module (see Rousseau et al. (2014a) for details) transfers information to the geotechnical module regarding the physiological plant properties that can

13

influence the mechanical properties of the river bank: depth and radius of rooting zone; cohesion owing to roots; trunk height, spacing, and diameter. The plant evolution module also includes functionalities to generate a plant cover and manage plant growth. In this study, however, dry mesh nodes were covered with trees from a single species associated with a single set of physiological properties that remained constant in time.

3. Method

3.1. Field data

The model is evaluated against hydrological and morphological data collected along a 1.5-km-long reach of the semialluvial river Medway Creek, London, Ontario (Fig. 3). Within this site, three zones were examined more closely owing to signs of previous erosion episodes; these zones will be referred to as A (transects 746-827), B (transects 352-409), and C (transects 929-954). The 20-m-wide channel is in a post-glacial valley covered by diverse assemblages of deciduous and coniferous trees, shrubs, and herbaceous species. The density of mature trees within the riparian area is higher in zone A. In zone B the tree density is noticeably lower and the proportion of shrubs higher, perhaps because of their proximity to an area that is seasonally flooded and occupied by beavers. Zone C includes mature trees between transects 932 and 940, but grass and shrubs in the downstream transects. Bank height along the external bends typically varies between 2 and 4 m, with two bluffs substantially increasing this value locally to 20 m (Fig. 3). This stream was selected because of the substantial observed erosion along certain banks but also because its flow has been monitored for decades. Bankfull discharge (1.5-year recurrence interval, based on gauging station 02GD008 just downstream of the study reach) is about 43 m³/s. In addition, sedimentology was examined by N. Bergman (personal communication, 8 December 2013) and rendered available for this project. Basic flow measurements (depth and velocity) were taken along the inlet and outlet cross sections of the study reach at low stage for the purpose of calibrating the flow and the energy slope prior to running numerical simulations. The difference between the predicted increase in free surface elevation at the outlet (1.58 m) from low (1.15 m³/s) to high flow discharge (60 m³/s) was

<7% compared with data from the gauging station (1.48 m), which is an acceptable error that is not expected to have an effect on the geotechnical modelling outcome of predicted river bank failures.
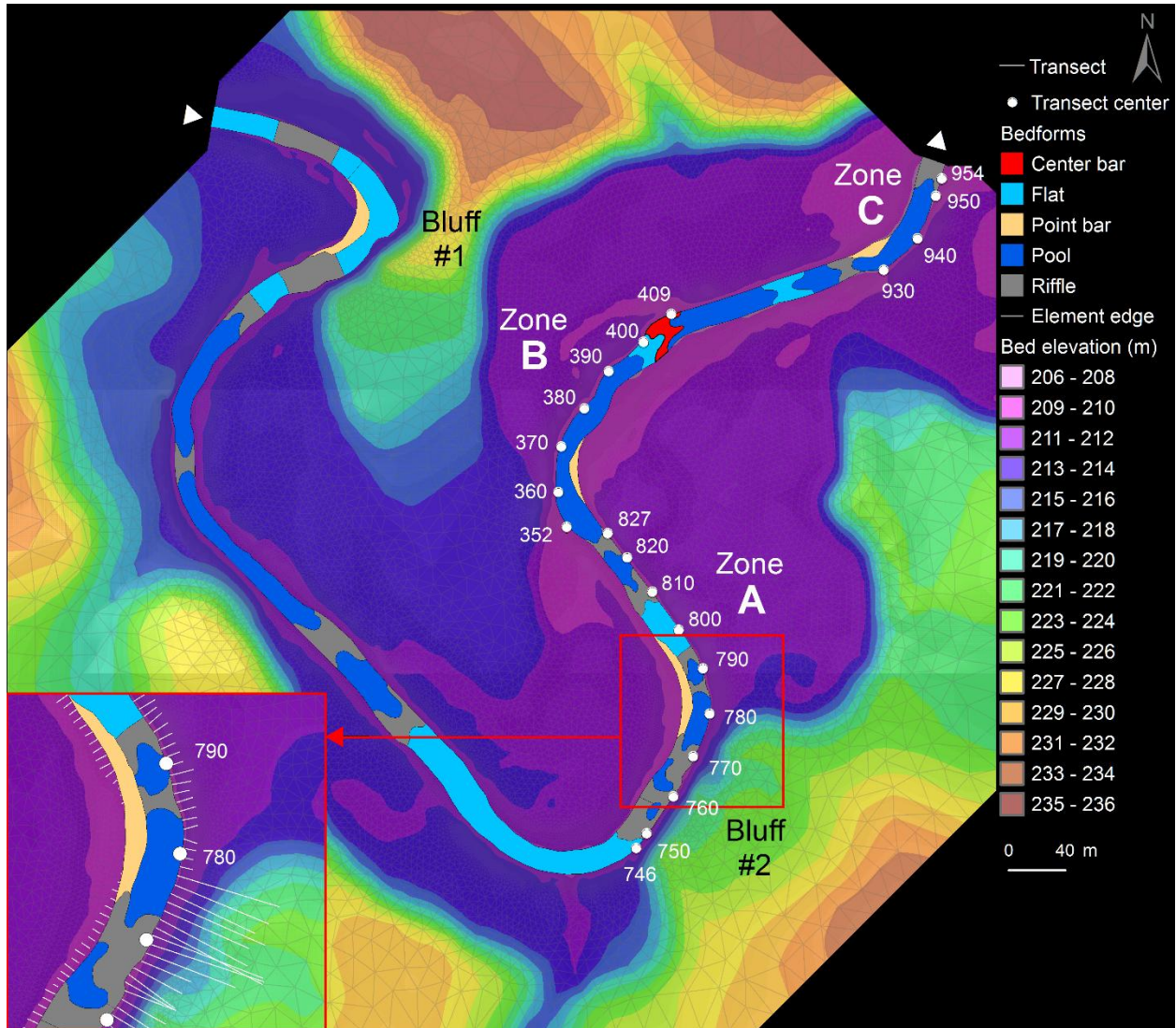
Fig. 3. Topography of the river and floodplain at Medway Creek, London, Ontario. The outline of computational elements appears in light grey. Three zones were studied in greater detail: zone A (transects 746-827), zone B (transects 352-409), and the downstream zone C (transects 929-954). The two white arrows indicate the position of liquid boundaries and flow direction. Bedform types correspond to the locations where the substrate was sampled by N. Bergman (personal communication, 9 June 2016). Note that the center bar is partially covered with long grass and shrubs. Inset: Detail on transects that are used in slope stability assessments for zone A.
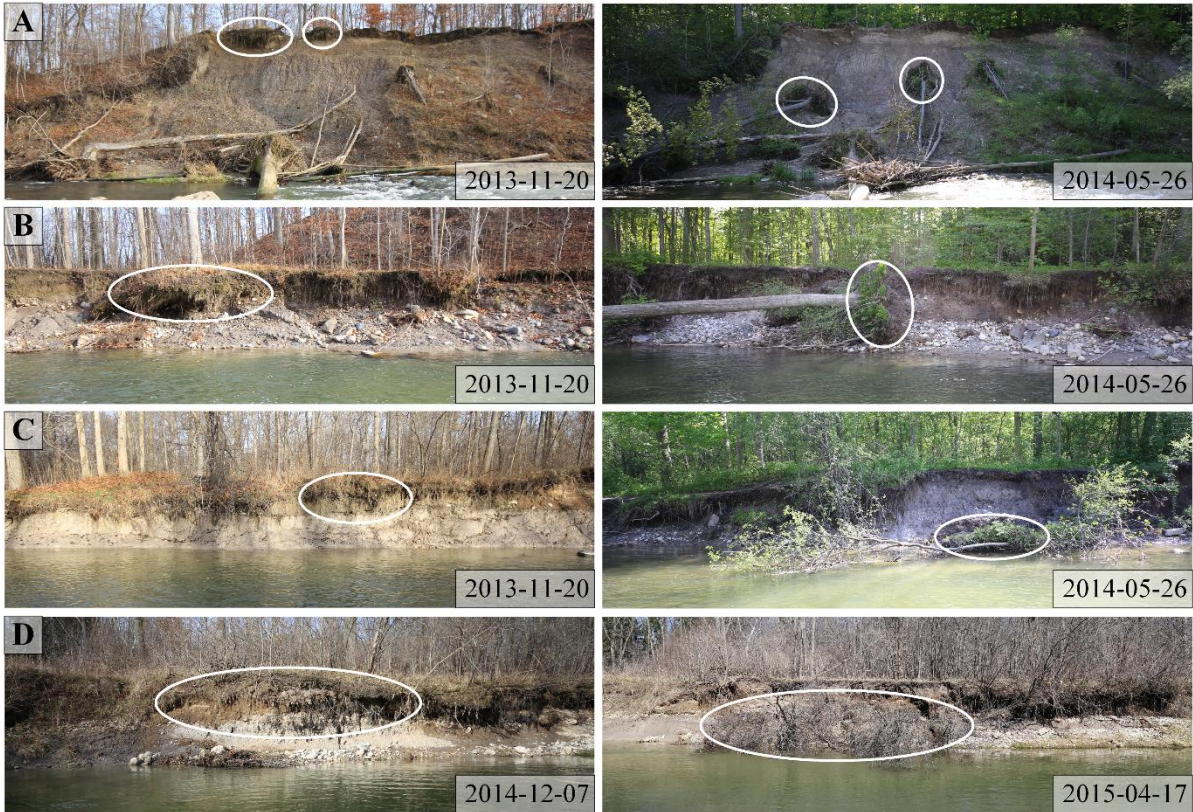
Fig. 4. Photographs of the most unstable river banks along the study reach between January 2012 and June 2015, before and after failure. The corresponding transects in Fig. 3 are (A) 760, (B) 781, (C) 807, and (D) 393-397. White ellipses highlight trees fallen owing to bank erosion.

Substantial efforts were put into surveying and monitoring channel morphology in this study. In November 2012, we collected over 5000 topography points of the channel bed and banks in the study reach using a differential GPS (resolution of 1 cm vertically and 1.5 cm horizontally). These points were combined with a 1-m resolution LiDAR digital elevation model (DEM) (The University of Western Ontario, 2006) to create a DEM of the channel and floodplain. Photographs of the banks were taken after each flood with discharge $Q \geq 15$ m³/s between February 2012 and April 2015 when the river banks were visible (e.g., no snow cover, no high flow) (Fig. 4). A consumer-grade camera with geotagging capabilities (Canon 60D) with wide-angle lens (Canon 10-20 mm) was employed along three banks that appeared unstable. A Garmin eTrek Legend CX hand-held GPS, mounted on the camera's hot shoe, recorded the position of each photograph. Photogrammetry analysis was performed on seven photograph sets taken in zone A (Fig. 3), corresponding to flooding events recorded between September 2013 and

16

April 2015 (Figs. 4, 5), in an attempt to estimate the amount of bank retreat in a nonintrusive way as the research site is located in a protected area. Targets were placed on six trees along unstable reaches to facilitate the analysis in the photogrammetric software Agisoft PhotoScan. Two of these trees were subject to bank failures and were evacuated by subsequent floods (Fig. 4B), which rendered the photogrammetry analysis more tedious and less accurate than expected. Although photographs were taken in zones B and C, photogrammetry was not attempted owing to the lack of bank retreat in these zones. The photogrammetry analysis reveals a bank retreat up to 2.4 m in zone A, which is compatible with visual cues (Fig. 4).
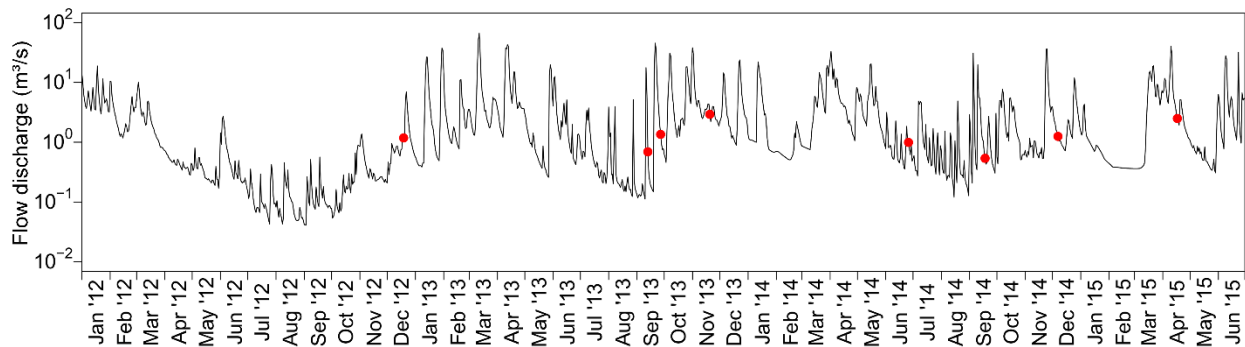
Fig. 5. Flood hydrograph between January 2012 and June 2015 based on gauging station 02GD008 located just downstream of the study reach. Red dots indicate the dates where measurements of bank morphology and characterization of bank condition took place.

Data acquired by N. Bergman (personal communication, 9 June 2016) in the same study reach revealed substantial spatial variations in grain size distribution (GSD) and various bedform types (riffles, pools, bars, flats, steps, and bluffs) (Fig. 3). Trial simulations, using a unique grain size distribution to describe bed substrate in the whole study reach, indicated the importance of varying GSD spatially. With a single curve, pools quickly filled with sediment, leading to a homogeneous longitudinal and lateral bathymetry very different from field observations. In order to simplify our simulations, grain size distribution data were reorganized into three classes using the package 'rPart' (Therneau et al., 2015) in the software R (R Core Team, 2013). The resulting GSD used in the simulations is presented in Table 1.

River banks exhibit three distinct soil layers along the study reach. The lower part consists of glacial till, which is buried under an equally thick sand layer and covered itself by a thin organic layer with dense

root network. However, in the absence of accurate sedimentological data for our study site, and for simplicity, we set up our model with uniform textured bank material with a single layer corresponding to the USCS class ML (silt, given a mean grain size diameter of 0.0234 mm). By doing so, we hypothesize that the lower layer is more resistant than the middle and upper layers and, thus, that the till determines bank strength and retreat, which is compatible with field observations.

Table 1
Grain size distribution curves

Category	Pool		Riffle		Flat		Step		Bar	
	Size (mm)	Fraction (%)	Size (mm)	Fraction (%)	Size (mm)	Fraction (%)	Size (mm)	Fraction (%)	Size (mm)	Fraction (%)
Fine	4.1	35	20.9	27	5.0	20	20.5	17	3.0	28
Medium	66.9	43	96.6	29	57.7	43	98.1	22	63.4	49
Coarse	271.2	22	250.9	44	189.0	37	270.3	61	239.7	23

3.2. Numerical setup

3.2.1. Mesh generation

The size of the triangular elements of the numerical mesh varied spatially to use a higher resolution in areas most likely affected by mass wasting (along steep river banks in bends) and on the channel bed to ensure that the simulated flow was grid independent. A moderate resolution was selected for the floodplain, and a low resolution for the valley walls. Grid-independence sensitivity analyses were completed to determine the appropriate number of nodes to include in the simulation domain (Roache et al., 1986; Lane et al., 2005; Biron et al., 2007). The number of mesh nodes was 67,780 (0.09 m²/element), 18,841 (1.20 m²/element), 17,003 (3.67 m²/element), and 4135 (48.69 m²/element) respectively in the steep-bank, bed, floodplain, and valley side zones. The time step was set to 0.1 s to ensure a Courant number close to unity.

3.2.2. Calibration and boundary conditions

Flow: A fixed-flat-bed simulation was first run with a low flow discharge of $Q = 1.15$ m³/s to adjust the elevation of the water surface at the inlet of the simulation domain to the measured inlet value at Medway Creek. This was done by varying bed roughness coefficient; a Strickler-Manning (n) value of 0.039 was selected for the entire bed. This procedure, which is common in CFD modelling (e.g., Bates et al., 1997; Rameshwaran et al., 2013), allows adjustment of the energy slope to fit experimental measurements (Vidal et al., 2007). At the field site, high-magnitude flooding events generally last a few days. For instance, a 66.2 m³/s peak discharge occurred during a flood event that lasted nearly six days. A time-contracted γ-distributed hydrograph was therefore fitted to the gauging station data to capture the intensity and shape of this event while limiting simulation length to 12 hours. The γ equation is given by

$$Q_t = Q_0 + (Q_P - Q_0) \cdot e^m \cdot \left(t/t_P \right)^m \cdot e^{-mt/t_P} \tag{12}$$

where Q_t = flow discharge at time t, Q_0 = initial discharge, Q_P = peak discharge, m = shape parameter, and t_P = peak time. In all simulations, parameter values were $Q_0 = 7.5$ m³/s, $Q_P = 60$ m³/s, $m = 4.8$, and $t_P = 3$ h.

Sediment: A mobile-bed simulation with fixed banks and steady bankfull discharge ($Q = 43$ m³/s) was run to determine the transport equations and substrate properties. The friction angle of the sediment was 36.5°, bed porosity 0.4, and mass density of sediment taken as 2650 kg/m³. This simulation revealed a stable bed with minor adjustments over a 24-hour period. During all simulations, the sediment rate at the inlet was equal to the outlet rate.
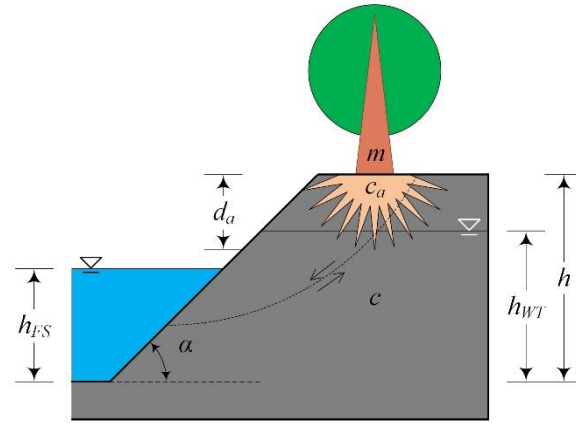
Fig. 6. Simplified bank profile and variables for the evaluation of model behaviour. Sensitivity analysis was conducted for the following variables: bank angle (°) and height (h), soil cohesion (c), height of free surface (h_{FS}) and water table (h_{WT}), trunk mass (m), apparent cohesion owing to roots (c_a), and root crown radius (d_a). The dotted arc represents a hypothetic slip surface.

Geotechnical slope stability and vegetation: Calibration was done in three ways. First, a series of bank stability predictions along a river bank with a simple profile (Fig. 6) was undertaken to explore model behaviour for a range of biophysical conditions, to identify the most sensitive variables, and to estimate parameter values to use in subsequent 3D simulations. For the evaluations that included vegetation effects, a single Sugar Maple (species) tree located at the bank top was considered. This tree was assumed to be positioned on the slump block, thus increasing the weight of a slump block intersecting bank top. Tree length and root radius were calculated from trunk diameter using empirical equations presented in Kenefic and Nyland (1999) and Tubbs (1977), respectively for length and radius. Wood density was assumed to be 690 kg/m³ (Green et al., 2007). The range of parameter values considered for each sensitivity analysis (geotechnical and geotechnical- vegetation) covered those found at the field site. Owing to the nonlinearity of Eqs. 3-4 and stochastic behaviour of the genetic algorithm, results were analyzed using machine learning algorithms in R (R Core Team, 2013). The importance of variables was quantified using the 'randomForest' package (Breiman et al., 2015), whereas classification trees were built using the 'rPart' package (Therneau et al., 2015). In the latter analysis type, tree complexity was selected in such a way that the standard error be

20

Table 2

Parameters of the geotechnical model

Properties of bank material	
USCS class	ML
Mean grain size (mm)	0.0234
Cohesion (kPa)	0.25
Compaction	75%
Transects	
Length (initial; minimum) (m)	5.0; 1.0
Number of nodes (initial; additional on bank top)	65; 3
Number of mesh nodes and trial angles during orientation	9; 33
Stability assessment	
Minimum block width (% of transect length)	75.0
Minimum block profile area (m²)	$1 \cdot 10^{-2}$
Number of vertical block slices	2^5
Safety factor precision; mass balance precision (m³)	$1 \cdot 10^{-4}$
Mass balance precision (m³)	$1 \cdot 10^{-4}$
Genetics	
Population size	48
Number of generations (minimum; maximum)	16; 32
Number of generations without improvement (maximum)	4
Mutation rate (%)	12.5
Migration rate (%)	65.0
Options: Inbreeding; polygamy	no; no

smaller than the error difference between consecutive levels of complexity. Second, a series of one-iteration mobile bed-and-banks simulations was completed to help determine the value of key geotechnical parameters: cohesion, USCS class, mean grain size, and compaction. The objective was to ensure that no mass failure occurs for a set of parameters representing the (low) flow conditions encountered during the week when the initial channel survey was completed. Bank stability was found to be sensitive to the four parameters with the exception of compaction. The parameter values that produced the fewest failures were selected (Table 2). Third, a series of 2:45 hour-simulations (corresponding to the peak values of the γ-distributed curve representing the hydrograph) were run to further examine the model's sensitivity to soil cohesion. Although the geotechnical module has the capability to calculate soil

Table 3

Parameters varied during numerical simulations; trunk spacing is equal to twice rooting depth d_a

| Configuration	Vegetation parameters					
	a_{TREE}	d_{BASE}	h_{TREE}	m_{TRUNK}	d_a	c_a
HYD	-	-	-	-	-	-
SED	-	-	-	-	-	-
GTC	-	-	-	-	-	-
RVG$_{SMALL}$	12.5	8.7	12.1	25	1.00	0.025
RVG$_{MEDIUM}$	23.2	20.9	21.1	250	1.25	0.250
RVG$_{LARGE}$	50.3	55.7	29.8	2500	1.75	1.250

Legend: HYD = a hydraulic-only simulation; SED = a HYD simulation with sediment transport; GTC = a SED simulation with mass wasting; RVG = a GTC simulation with a single tree type of size specified in the subscript; a_{TREE} = tree age (years); d_{BASE} = basal trunk diameter (cm); h_{TREE} = tree height (m); m_{TRUNK} = trunk mass (kg); d_a = rooting depth (m); and c_a = apparent cohesion due to roots (kPa).

cohesion based on USCS class and degree of saturation, we note a substantial discrepancy between the range of bank cohesion values typically encountered in nature (9-67 kPa for USCS class ML) and those employed while calibrating the geotechnical module (0.25-1.50 kPa). Thus, this variable should be considered as a numerical parameter rather than an input variable, in a similar way to the roughness coefficient for hydrodynamic calibration. The high degree of compaction was assumed to match the geological past of this post-glacial environment. Regarding bank hydrology, water table elevation adjustment rates k of 0.056 and 0.018 were used respectively for the rising and falling limbs of the hydrograph. These values were obtained by fitting Eq. 7 to data acquired by Needelman (2013) in a river bank of similar composition. The values assigned to key parameters of the genetic algorithm are provided in Table 2. These parameters were adjusted to minimize computation time whilst maximizing precision.

3.3. Simulations and analysis procedure

Excluding the calibration simulations, a total of six simulations were run with the biophysical parameters described listed in Tables 2-3. Physiological plant properties were varied in a way as to provide a range of stabilization power; threshold parameter values were estimated using machine learning algorithms applied to the output of geotechnical slope stability assessments along a simplified river bank profile. A high

value of apparent cohesion c_a was attributed to a large, 50-year-old Sugar Maple tree, whilst the value

assigned to small and medium trees was proportional to the basal trunk area of the large tree.
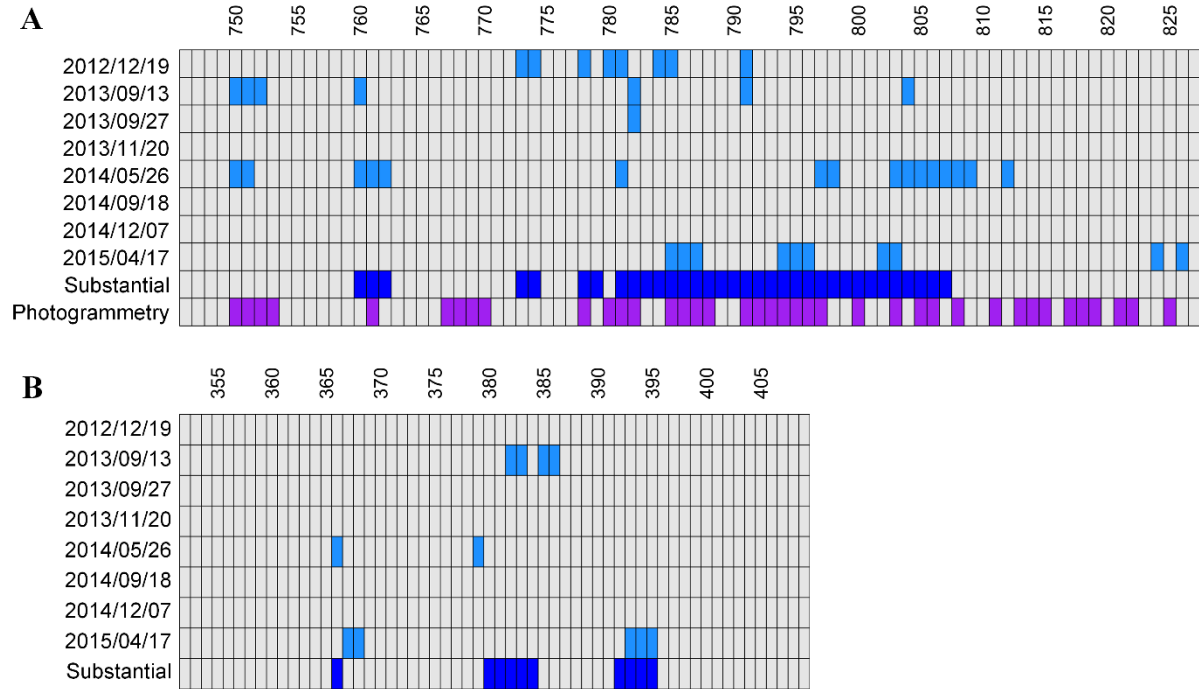
Fig. 7. Occurrence of river bank failures along zones A and B based on photographs. A light blue box corresponds to an observed geotechnical failure for a specific date and transect. Dark blue boxes correspond to substantial total retreat ($\geq$0.1 m^2) during the observation period, i.e., between 19 December 2012 and 17 April 2015, and include fluvial and geotechnical processes that led to the removal of bank material along a transect. Purple boxes indicate transects where retreat was detected by photogrammetry for the same period (provided for zone A only).

4. Results

4.1. Field observations

A total of 25 flooding events with a magnitude of $Q \sim 15$ m³/s or above were recorded during the study

period (2012-2015) (see Fig. 5). The largest number of bank failures were noticed on 26 May 2014,

following a winter that included six floods with peak discharge varying between 14.4 and 33.0 m³/s and

after receiving 45.3 mm of rain, and on 17 April 2015 (associated with 18.9 and 40.3 m³/s floods). Zone

A was subject to a larger number of failures (42) than zone B (11) (Fig. 7), whereas a single minor failure

occurred along transect 953 of zone C on 20 November 2013 (not shown). Photogrammetry analysis

performed for zone A of the study reach reveals a bank retreat up to 2.4 m in the eroded areas (purple

column in Fig. 7). Assuming that bank evolution occurred where calculated retreat rates were ≥10 cm, the accuracy of photogrammetric measurements, relative to field observations, was 61%; this low value is owing to a low number of benchmarks. In addition, riparian vegetation is responsible for false positives downstream of transect 812. The accuracy climbs to 76% when excluding these transects. Nevertheless, the magnitude of retreat rates is comparable to visual observations made in the field.

4.2. Accuracy quantification and evaluation

In order to facilitate the comparison of numerical simulations with morphological changes observed at the field site, the accuracy of each prediction was quantified using Youden's (1950) index:

$$J = SN + SP - 1 = \frac{TP}{TP + FN} + \frac{TN}{TN + FP} - 1 \tag{13}$$

where SN = sensitivity, SP = specificity, TP = number of true positive, TN = number of true negatives, FP = number of false positives, and FN = number of false negatives. This rating method provides a constant range of indices, between 1.0 (correct prediction for every transect) and -1.0 (wrong prediction for every transect), which facilitates the comparison of predictive accuracy amongst configurations and river reaches. In our analysis, an error of one transect spacing (~3.5 m) is tolerated, which means that a prediction contributes to TP if a failure was observed along a given transect or along its directly neighbouring transects.

4.3. Effects of model components

4.3.1. Hydraulics

Given the scoring system described above, using maximum bed shear stress along a channel cross section as an indicator of bank evolution is not very successful. Indeed, using a threshold value of 25 Pa results in Youden's indices of -0.28 and -0.15 respectively for zones A and B (rows HYD in Fig. 8). This threshold value was selected because it maximizes the overall accuracy of hydraulic simulations. Very few failures are correctly predicted (true positives), and several are incorrectly predicted (false positives).

24
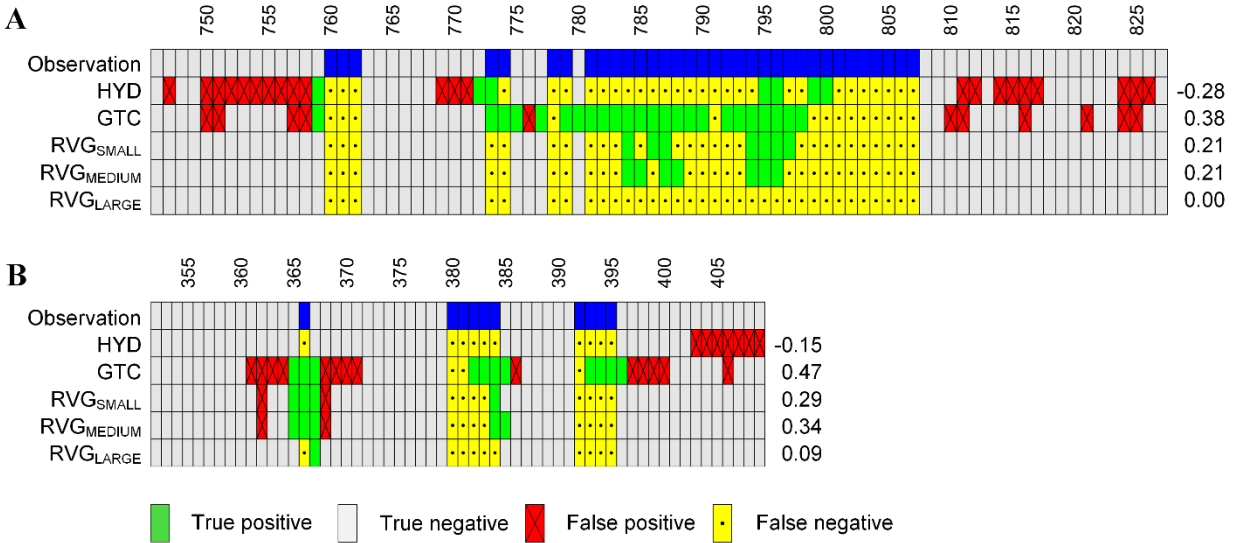
Fig. 8. Comparison of bank failures observed within the study reach between January 2012 and June 2015 to numerical predictions. The *x*-axis labels correspond to the transects shown in Fig. 3 for zones A and B. Zone C is not shown owing to the lack of substantial bank retreat through mass wasting during the observation period. The values on the right side of each table correspond to Youden's index attributed to each numerical prediction, calculated using Eq. 13. The observation row corresponds to the substantial row in Fig. 7. HYD = a hydraulic-only simulation; GTC = a simulation with sediment transport and mass wasting; RVG = a GTC simulation with a single tree type of size specified in the subscript. The subscripts SMALL, MEDIUM, and LARGE refer to tree size (see Table 3 for the physiological properties of plant cover).

4.3.2. Sediment transport

The result of the simulation with bedload transport only, i.e., with the geotechnical and vegetation modules disabled, reveals a fairly stable channel with changes located primarily along channel margins. Nevertheless, looking at the total volume of displaced material, we note an initial adjustment of bed morphology during the first iteration of the simulation followed by a slow evolution rate that is proportional to flow discharge during the rising and falling limbs of the hydrograph. Insignificant bathymetric changes, combined with rapid channel stabilization, indicate that the coupled morphodynamic model Telemac2D-Sisyphe, i.e., without geotechnical algorithms, is unlikely to simulate lateral retreat in our study reach.

4.3.3. Geotechnical processes

Simulations with different parameter sets were run to evaluate the sensitivity of the coupled geotechnical model to key parameters. For instance, doubling the adjustment rate of the water table elevation results in very similar erosion patterns. However, a rise in water table elevation within the river bank is required to create mass wasting in the upper bluff area. Although a steady low flow discharge of 7.5 m³/s is sufficient to trigger the retreat of low banks, a peak discharge of 60 m³/s, i.e., similar to the maximum value recorded during the observation period (66.2 m³/s on 12 March 2013), when combined with a γ-shaped hydrograph curve, improves fit with observations. In particular, a flow discharge of 60 m³/s affects the tall bluff (transects 746-762 in Fig. 3) and increases the length of the eroded bank subject to mass wasting (transects 778-807 in Fig. 8A). Similarly, soil cohesion values of 0.25, 0.50, and 1.00 kPa were evaluated, with a value of 0.25 kPa resulting in the best match with field observations.

Enabling the geotechnical module results in much improved predictions of retreat location compared to using a threshold bed shear stress value. This is reflected in the calculated accuracy values, i.e., Youden's indices of 0.38 (GTC) vs. -0.28 (HYD) in zone A, and 0.47 vs. -0.15 in zone B (Fig. 8B). Despite the presence of several false positives, configuration GTC correctly predicts the location of the river banks where acute erosion was observed in the field (row GTC in Fig. 8). Two of the most unstable bank regions along zone A are correctly identified (Figs. 4A-B). The model may not be able to identify transects 799-807 (Figs. 4C and 8A) because most failures along this bank occurred only once the upstream 50-m region had retreated substantially, i.e., after 18 floods with a magnitude of at least 15 m³/s over a period of 1.5 years (Fig. 7). Although configuration GTC results in the largest number of true positives, it also involves several false positives between transects 810-825 (Fig. 8A). This may be explained by the fact that the presence of riparian vegetation is only indirectly, partially accounted for with an adjustment of soil cohesion in configuration GTC.

4.3.4. Riparian vegetation

The vegetation module developed for this study influences the degree of bank stability by increasing soil cohesion (up to a certain depth under soil surface, depending on plant physiology) and by increasing the mass of a slump block (tree species only). These mechanical actions in turn affect friction forces along the slip surface (e.g., dashed line in Fig. 1A), stabilizing or destabilizing a river bank, depending on bank geometry and local biophysical conditions.

All three configurations involving vegetation, i.e., RVG_{SMALL}, RVG_{MEDIUM}, and RVG_{LARGE}, induce a drastic reduction in the number of failures (false positives and true positives) relative to the basic geotechnical scenario (row GTC in Fig. 8). Configurations with small and medium trees result in Youden's indices lower than that of the GTC configuration in zone A. Although this difference is less important in zone B, configurations RVG_{SMALL} and RVG_{MEDIUM} fail to predict the correct extent of the large unstable zone (transects 778-807 in Fig. 8A) and the occurrence of failures in the top of the bluff (Fig. 4A and transects 760-762 in Fig. 8A). In addition, the largest failure (in volume) recorded in zone B during the observation period is not predicted by the model (transects 392-395 in Fig. 8B). This may be caused by the increased stability in the model that was using trees, whereas at the field site for this zone shrubs are present. The scenario with the largest trees almost completely eliminated bank instabilities,

Table 4
Number of failures and absolute volume change in zones A, B, and C of the study reach; zone A corresponds to transects 746-827, zone B to transects 352-409, and zone C to transects 929-954 (Fig. 3)

Configuration	Number of failures			Volume change (m³)		
	A	B	C	A	B	C
SED	-	-	-	17.3	7.6	15.9
GTC	590	199	108	3316.7	352.8	45.7
RVG_{SMALL}	199	100	166	64.1	255.5	65.2
RVG_{MEDIUM}	108	94	151	51.9	138.3	41.1
RVG_{LARGE}	0	6	1	12.2	12.3	18.3

Legend: SED = a hydraulic simulation with sediment transport; GTC = a SED simulation with mass wasting; RVG = a GTC simulation with a single tree type of size specified by the subscript.

with a progression in mechanical reinforcement with an increase in tree size. Although vegetation considerably reduces the number of failures and volume of displaced floodplain material, it does not necessarily reduce the mean failure volume (Table 4). For instance, 151 failures produced a total displacement of 41.1 m³ in zone C under the RVG$_{MEDIUM}$ configuration, whereas a single failure displaced 18.3 m² under RVG$_{LARGE}$. Therefore, vegetation cover triggers a nonlinear response that seems to be
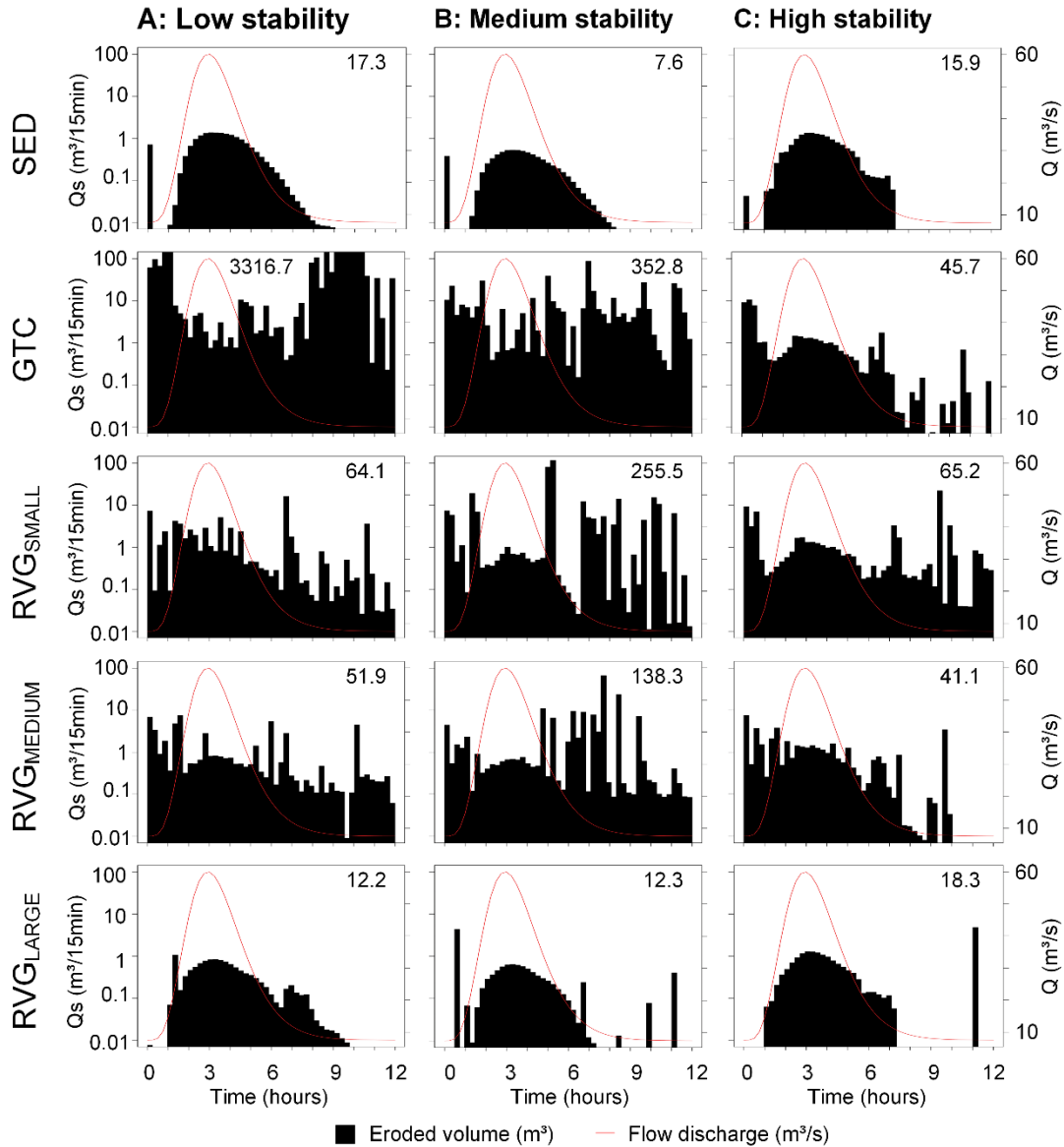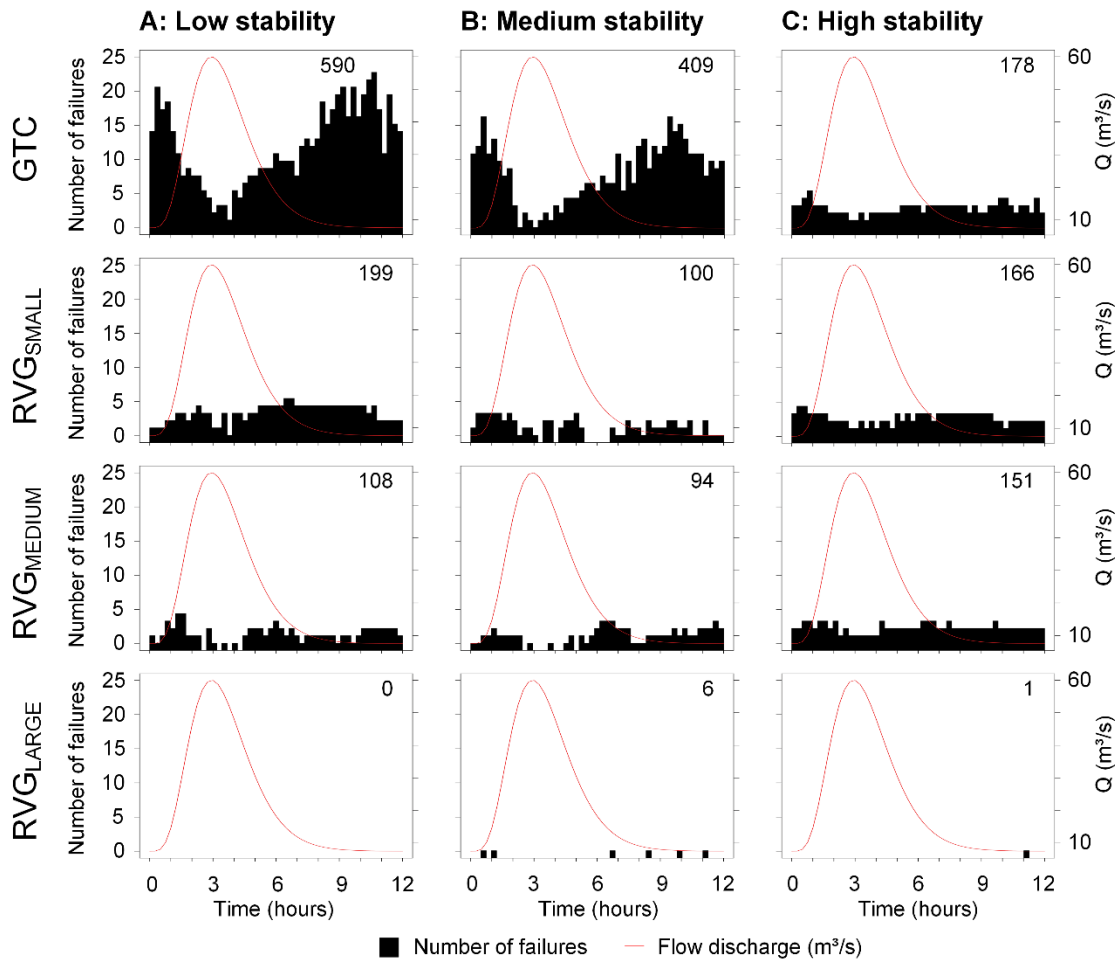

Fig. 9. Floodplain material displacement (Q_s on the primary *y*-axis) and flow discharge (Q on the secondary *y*-axis) during numerical simulations as a function of simulation time. Columns correspond to zones A (low bank stability), B (medium bank stability), and C (high bank stability) in Fig. 3. In-plot annotations are the cumulative, simulated displaced volumes (m³).

28

exacerbated by complex river bank geometry, combined with the stochastic nature of the genetic algorithm. Nonlinearity is expected to increase even more with spatiotemporal variations in sedimentology and in plant physiology and assemblage.

4.4. Timing and magnitude of bank retreat

Neglecting soil displacement occurring at the onset of simulations (which may be attributed to bed adjustment with respect to flow dynamics), the SED configuration produces displacement rates matching the shape and phase of the γ-distributed hydrograph, with maximum values reaching 1.3, 0.6, and 1.4 m³/15-min period respectively for zones A, B, and C (Fig. 9). Activating the geotechnical module

Fig. 10. Number of failures (on the primary *y*-axis) and flow discharge (*Q* on the secondary *y*-axis) during numerical simulations as a function of simulation time. Columns correspond to zones A (low bank stability), B (medium bank stability), and C (high bank stability) in Fig. 3. In-plot annotations are the total number of simulated failures.

alters the timing of mass wasting and total volume of displaced soil material, and produces a complex signal emerging from the overlap of bedload entrainment and mass wasting processes. Although we note similar patterns in the geomorphic response to the 12-hour flood event amongst zones and amongst configurations (Fig. 9), displacement occurs primarily near the end of the falling limb, i.e., when flow discharge has returned to preflood magnitude. The lag between flow and soil displacement peaks seems to be caused by the indirect consideration of soil hydraulic conductivity in the geotechnical modules, which is done by defining water table convergence coefficients. The similarity in response between zones A and B (Figs. 9-10) may be attributable to similarities in bank geometry, height, and cover along unstable transects. In particular, zone C has a lower tree density than zones A and B and does not exhibit three distinctive soil strata. Finally, note that a substantial reduction in the number of failures does not automatically translate into a substantial reduction in the volume of displaced soil material (e.g., Fig. 9 vs. Fig. 10).

The volume of displaced soil material is inversely proportional to the maturity of the vegetation cover, which demonstrates the substantial contribution of physiological plant properties on channel dynamics (Fig. 9). Small and medium trees reduce the incidence of mass wasting in zones A and B but have very little effect in zone C (Fig. 10). Note that a patch of young trees provides enough soil reinforcement to substantially reduce the number of failures. The timing of displaced material in configuration RVG_{LARGE} is similar to the timing in SED, with the distinction that vegetation slightly reduces soil displacement rate (Fig. 9). This may be attributed to the increase in friction caused by the presence of riparian vegetation on river banks, which highlights the importance of including flow-vegetation interaction.

5. Discussion

This research confirms that a morphodynamic model lacking a dedicated geotechnical component is unable to simulate lateral adjustments in a meandering channel with cohesive banks. In our simulations, the sediment transport module alone predicts little bank retreat for a study reach that was observed to be

unstable. In addition, using a threshold bed shear stress value appears to be a weak predictor for the location of bank failures (row HYD in Fig. 8).

Lateral erosion processes have been included into fluvial models using various approaches, and comparing them directly with the modules presented here is not straightforward, particularly as very few have attempted to simulate complex natural cases (e.g., Van de Wiel and Darby, 2004). Bishop's (1955) method of slices, used here to quantify river bank stability, was also employed in other fluvial studies, but often with the intent of examining the geotechnical stability at the river bank and reach scales, not connecting it to a hydraulic model (e.g., Van de Wiel and Darby, 2007; Langendoen and Simon, 2008; Midgley et al., 2012). A few models consider geotechnical soil properties in the calculation of retreat rates, but these are generally kept constant during a simulation. For instance, the incipient collapse angle is not affected by flow stage in Asahi et al. (2013).

A major advantage of our model is the integration of a river bank hydrology module and the consideration of spatial variations in soil moisture within the bank during stability evaluations. Furthermore, it allows the complexity of natural rivers to be fully represented, whereas most other models impose idealized bank profiles (e.g., Eke et al., 2014; Langendoen et al., 2016) and planform geometries (e.g., Crosato, 2007). Several of these implementations assume (without enforcing) mass conservation during bank retreat and, by doing so, ignore the role of basal control on river bank stability (Thorne, 1982). However, retreat models incorporating a deposition algorithm exist (e.g., Van de Wiel and Darby, 2004; Dulal et al., 2010).

A major advantage of the proposed model is its genetic algorithm, which selects the failure mechanism (rotational or translational) as it determines the extent of the slump block. This feature is particularly relevant to the study of meandering river channels, which develop in cohesive floodplains (Anderson and Anderson, 2010), as rotational failures tend to be associated with cohesive soils (Thorne, 1982). Conversely, most existing bank retreat formulations assume noncohesive soils, and therefore translational failures. The consideration of biophysical conditions (e.g., soil composition and moisture,

31

flow stage, water table elevation, plant cover) by the genetic algorithm is also compatible with the episodic nature of bank retreat in natural rivers (Abernethy and Rutherfurd, 1998; Pollen-Bankhead and Simon, 2010). Therefore, existing morphodynamic models, often generating geometrically idealized meandering planforms, may not apply to complex river environments.

Bank retreat along Medway Creek was discontinuous in time, space, and magnitude during the observation period (Figs. 7 and 8). These irregularities are fairly well simulated by our model, which seems to suggest the necessity to include a sophisticated geotechnical algorithm in morphodynamic models for improved applicability to natural rivers. The proposed modelling approach, which is more detailed and physics-based than previous implementations in the description of salient processes, therefore reduces the gap between theory and practical applications for complex river environments by integrating vector-based geospatial treatment, not only in data surveying as Güneralp and Marston (2012) suggest but at the heart of the modelling algorithm.

The integration of physics-based stability equations also facilitates the fragmentation of river bank erosion into distinct processes (e.g., fluvial and geotechnical), forces (e.g., hydrostatic pressure, pore-water pressure, slump block weight), and components (e.g., riparian plants). Fragmentation, which is one of the key novelties of the proposed morphodynamic modelling approach, enables to examine causal relationships, with parameter values defined in terms of distinct, ideally measurable, physical quantities. Existing planform meander models, including the HIPS formulation (Hasegawa, 1977; Ikeda et al., 1981), simulate lateral retreat as a function of excess near-bank shear stress or excess velocity (e.g., Güneralp et al., 2012; Zolezzi et al., 2012), which prevents the direct manipulation of variables influencing lateral erosion.

A similar observation can be made regarding the inclusion of plant effects. Most existing models indirectly consider vegetation (but see Van de Wiel and Darby (2004, 2007) for a simplified physics-based approach) by increasing the threshold stream power required to initiate sediment transport (e.g., Murray and Paola, 2003) or by altering bed roughness based on plant physiology and arrangement, which

reduces near-bed velocities (e.g., Crosato and Saleh, 2011), or by attributing an added cohesion value owing to presence of roots while ignoring surcharge effect (e.g., Eaton and Giles, 2009). Fuzzy concepts have also been used to lump, quantify, and integrate the stabilization effects of riparian plants. Modifying bank erodibility based on biomass density (e.g., Camporeale et al., 2013) allows to relate planform patterns to biomass density and vegetation growth rate (Perucca et al., 2007). However, this numerical, immaterial, and partially subjective conceptualization of floodplain vegetation limits the application of these models to real-world investigations as biomass does not unambiguously translate into a set of measurable physiological plant properties or alterations of soil strength.

By fragmenting geotechnical and vegetation processes and forces, the model presented in this paper facilitates the identification of causes of bank failure. However, the current version of the model fails to recognize the normal range of cohesion values associated with soil and roots in nature, which indicates that it is not yet capable of accounting for the overall complexity of the natural environment, although the overall approach constitutes a step in this direction.

Describing fluvial processes using physically correct equations considerably increases run time, and therefore, severely limits the spatiotemporal scales that can be investigated. The inclusion of the nonlinear version of the shallow-water equations and quantification of geotechnical stability based on a limit equilibrium method, combined with the selection of appropriate cell size and time step to ensure numerical stability and the validity of predictions (e.g., grid-independence testing using Biron et al. (2007); Courant number below unity), contribute to this situation. Despite the activation of parallel processing and the use of a genetic solver for the geotechnical computations, each simulation took ~4.5 days to run on a computer equipped with double hex-core processors. As an indication, the coupled model spent 18.0%, 69.5%, and 12.5% of its time in the hydraulic, sediment, and geotechnical modules respectively. Thus, further improvements in algorithmic efficiency are needed for river scientists and practitioners to employ the type of model presented here to perform simulations over long spatiotemporal scales.

In this study, and for the sake of efficiency, we explored parameter sensitivity using machine learning algorithms on a series of one-iteration simulation results and identified threshold values for key parameters. Such short trial simulations helped to identify the range of reasonable parameter values but did not allow for the interaction between processes and the full spectrum of combinations of biophysical conditions to be taken into account. This may explain why activating the vegetation module enhances stability more drastically than expected, leading to less accurate predictions than a strictly geotechnical simulation. The outcome may have differed with a sophisticated calibration/fitting method capable of determining soil and apparent (owing to roots) cohesion values maximizing correlation between observed and predicted failures.

The proposed bank retreat approach differs from previous implementations in its enhanced applicability to complex natural river environments, as most geotechnical models simulating river banks failures are limited in scale to a few tens of meters (e.g., Thomas and Pollen-Bankhead, 2010; Midgley et al., 2012), whilst morphodynamic models mainly focus on flume-size channels with noncohesive banks (e.g., Langendoen et al., 2016) and assume nonvegetated floodplains (e.g., Pittaluga and Seminara, 2011; Asahi et al., 2013). Therefore, with a few exceptions such as the model developed by Lai et al. (2015), it is one of the very few models that can accurately predict bank erosion episodes at a scale relevant to the management and restoration of river reaches. Validating the meandering planform properties and dynamics predicted by pseudo-empirical approaches is often limited to a coarse comparison of behavioural evolutionary traits against those visible in historical aerial photographs (e.g., Camporeale et al., 2005; Perucca et al., 2007; Duan and Julian, 2010) or against data sets from analogue flume experiments (e.g., Duan et al., 2001; Rüther and Olsen, 2007). Conversely, the fairly subtle planform changes associated with physics-based models are not necessarily detectable on airborne imagery. Although a sophisticated, physics-based model applicable to natural vegetated rivers provides more detailed mechanistic information related to river bank erosion processes, it also requires exhaustive data measurements for parameterization and validation, which are seldom available.

6. Conclusion

New geotechnical and vegetation modules were developed and coupled to the hydrodynamic module Telemac-2D and sediment transport module Sisyphe to create a universal and more physics-based representation of the evolution of alluvial river channels at the kilometer scale. The agreement between observed and predicted river bank failures in our simulations is encouraging, and comparison with field data revealed a marked improvement in bank failure predictions when adding the geotechnical module, albeit with limited gain in accuracy when adding the vegetation module.

The main novelty of the developed modules is the possibility to parameterize lateral erosion using physical, measurable quantities such as geotechnical soil properties (texture, cohesion, compaction, and porosity) and physiological plant properties (wood density, trunk diameter and length, and root strength and depth). Importantly, and innovatively, the geotechnical evaluations are done independently of the hydrodynamic mesh, which allows single- or multithreaded alluvial river types of any scale (flume, stream, and river) to be studied for cohesive and noncohesive soils, with or without aquatic or terrestrial plants. The consideration of a floodplain rather than strictly a channel allows us to consider palaeochannels and to include the effects of mass wasting events occurring away from the channel, for instance, along valley walls. Furthermore, the effect of soil water content, in particular the effects of the imbalance between free surface and water table elevations during a flooding event, is an important addition to the model as it is recognized as critical to river bank stability. Finally, the use of a fully configurable genetic algorithm with tournament selection keeps runtimes close to those of a morphodynamic model lacking a lateral erosion algorithm while allowing to efficiently locate planar, circular, and noncircular slip surfaces through a single algorithm. Our solution addresses some of the critiques of existing morphodynamic models such as the lack of physics in lateral erosion algorithms, the omission of mass wasting and vegetation processes, and their incapacity to consider multithreaded channels.

35

To enhance the applicability of the developed model for river-related management issues, future developments should focus on improving the physical representation of vegetation, in particular, with respect to the cohabitation of multiple individuals and species in a single simulation cell, a situation that is usually encountered in a natural setting. An adaptive mesh, such as the one built by Langendoen et al. (2016), would also likely be more efficient for physics-based 2D and 3D models. Most importantly, there is a serious need for accessible time series of biophysical, hydraulic, topographic, and sedimentological data sets to calibrate and validate models such as ours. As highlighted by Rousseau et al. (2016), creating a central repository providing universal validation cases for morphodynamic modelling would be extremely valuable.

Acknowledgements

References

Abernethy, B., Rutherfurd, I.D., 1998. Where along a river's length will vegetation most effectively stabilise stream banks? Geomorphology 23, 55-75.

Anderson, R.S., Anderson, S.P., 2010. Rivers. In: Geomorphology: the mechanics and chemistry of landscapes. Cambridge University Press, Cambridge, UK, 380-421.

Asahi, K., Shimizu, Y., Nelson, J., Parker, G., 2013. Numerical simulation of river meandering with self-evolving banks. J. Geophys. Res. - Earth Surf. 118(1–2): 1-22.

Bates, P.D., Anderson, M.G., Hervouet, J.-M., Hawkes, J.C., 1997. Investigating the behaviour of two-dimensional finite element models of compound channel flow. Earth Surf. Proc. Land. 22, 3-17.

Bertoldi, W., Siviglia, A., Tettamanti, S., Toffolon, M., Vetsch, D., Francalanci, S., 2014. Modeling vegetation controls on fluvial morphological trajectories. Geophys. Res. Lett. 41, 7167-7175.

Biron, P.M., Haltigin, T.W., Hardy, R.J., Lapointe, M.F., 2007. Assessing different methods of generating a three-dimensional numerical model mesh for a complex stream bed topography. Int. J. Comput. Fluid. D. 21(1), 37-47.

Bishop, A.W., 1955. The use of the slip circle in the stability analysis of slopes. Géotechnique 5(1), 7-17.

Breiman, L., Cutler, A., Liaw, A., Wiener, M., 2015. randomForest - Classification and regression based on a forest of trees using random inputs [computer software]. R package version 4.1-10.

Camporeale, C., Perona, P., Porporato, A., Ridolfi, L., 2005. On the long-term behavior of meandering rivers. Water Resour. Res., 41(12), W12403.

Camporeale, C., Perucca, E., Ridolfi, L., Gurnell, A.M., 2013. Modeling the interactions between river morphodynamics and riparian vegetation. Rev. Geophys. 51(3), 379-414.

Chen, D., Tang, C., 2012. Evaluating secondary flows in the evolution of sine-generated meanders, Geomorphology 163-164, 37-44.

Collins, D.B.G., Bras, R.L., Tucker, G.E., 2004. Modeling the effects of vegetation-erosion coupling on landscape evolution. J. Geophys. Res. 109, 1-11.

Coulthard, T.J., Van de Wiel, M.J., 2006. A cellular model of river meandering. Earth Surf. Proc. Land. 31, 123-132.

Crosato, A., 2007. Effects of smoothing and regridding in numerical meander migration models. Water Resour. Res., 43, W01401.

Crosato, A., Saleh, M. S., 2011. Numerical study on the effects of floodplain vegetation on river planform style. Earth Surf. Proc. Land., 36, 711-720.

Darby, S.E., Alabyan, A.M., Van de Wiel, M.J., 2002. Numerical simulation of bank erosion and channel migration in meandering rivers. Water Resour. Res. 38(9), 1163.

Duan, J.G., Julien, P.Y., 2010. Numerical simulation of meandering evolution. J. Hydrol. 391, 34-46.

Duan, J. G., Wang, S.S.Y., Jia, Y.F., 2001. The applications of the enhanced CCHE2D model to study the alluvial channel migration processes. J. Hydraul. Res., 39(5), 469-480.

Dulal, K.P., Kobayashi, K., Shimizu, Y., Parker, G., 2010. Numerical computation of free meandering channels with the application of slump blocks on the outer bends. J. Hydro Environ. Res, 3, 239-246.

Eaton, B.C., Giles, T.R., 2009). Assessing the effect of vegetation-related bank strength on channel morphology and stability in gravel-bed streams using numerical models. Earth Surf. Proc. Land., 34, 712-724.

Egiazaroff, I.V., 1965. Calculation of non-uniform sediment concentrations. J. Hyd. Eng. Div. ASCE 91, 225-248.

Eke, E., Parker, G., Shimizu, Y., 2014. Numerical modeling of erosional and depositional bank processes in migrating river bends with self-formed width: morphodynamics of bar push and bank pull. J. Geophys. Res. Earth Surf., 119, 1455-1483.

El Kadi Abderrezzak, Die Moran, A., Tassi, P., Ata, R., Hervouet, J.-M., 2016. Modelling river bank erosion using a 2D depth-averaged numerical model of flow and non-cohesive, non-uniform sediment transport. Adv. Water Resour., 93, 75-88.

Evangelista, S., Greco, M., Iervolino, M., Leopardi, A., Vacca, A., 2015. A new algorithm for bank-failure mechanisms in 2D morphodynamic models with unstructured grids. Int. J. Sediment Res. 30, 382-391.

Fellenius, W., 1927. Statistical analysis of earth slopes and retaining walls considering both friction and cohesion and assuming cylindrical sliding surfaces. W. Ernst und Sohn, Berlin, Germany (in German).

Galland, J.-C., Goutal, N., Hervouet, J.-M., 1991. TELEMAC: A new numerical model for solving shallow water equations. Adv. Water Resour. 14(3), 138-148.

Green, D.W., Winandy, J.E., Kretschmann, D.E., 2007. Mechanical properties of wood. In: The Enyclopedia of wood [technical report]. U.S. Department of Agriculture. Skyhorse Publishing, New York.

Güneralp, I., Marston, R.A., 2012. Process-form linkages in meander morphodynamics: bridging theoretical modeling and real world complexity. Prog. Phys. Geog. 36(6), 718-746.

Güneralp, I., Abad, J. D., Zolezzi, G., Hooke, J., 2012. Advances and challenges in meandering channels research. Geomorphology, 163-164, 1-9.

Ham, D., Church, M., 2012. Morphodynamics of an extended bar complex, Fraser River, British Columbia. Earth Surf. Proc. Land. 37, 1074-1089.

Hasegawa, K., 1977. Computer simulation of the gradual migration of meandering channels. Proceedings of the Hokkaido Branch. Japan Society of Civil Engineering, pp. 197-202 (in Japanese).

Ikeda, S.G., Parker, G., Sawai, K., 1981. Bend theory of river meanders: 1. Linear development. J. Fluid Mech. 112, 363-377.

Iwasaki, T., Shimizu, Y., Kimura, I., 2016. Numerical simulation of bar and bank erosion in a vegetated floodplain: A case study in the Otofuke River. Adv. Water Resour. 93, 118-134.

Johannesson, H., Parker, G., 1989. Linear theory of river meanders. In: Ikeda, S., Parker, G. (Eds.), Water Resour. Monogr. 12. AGU, Washington, pp. 181-214.

Kenefic, L., Nyland, R.D., 1999. Sugar Maple height-diameter and age-diameter relationships in an uneven-aged northern hardwood stand. Northern Journal of Applied Forestry 16(1), 43-47.

Koch, F.G., Flokstra, C., 1981. Bed level computations for curved alluvial channels. XIXth Congress of the International Association for Hydraulic Research. New Delhi, India.

Lai, Y.G., Thomas, R.E., Ozeren, Y., Simon, A., Greimann, B.P., Wu, K., 2012. Coupling a two-dimensional model with a deterministic bank stability model. ASCE World Environmental and Water Resources Congress: Albuquerque, New Mexico.

Lai, Y.G., Thomas, R.E., Ozeren, Y., Simon, A., Greimann, B.P., Wu, K., 2015. Modeling of multilayer cohesive bank erosion with a coupled bank stability and mobile-bed model. Geomorphology 243, 116-129.

Lane, S.N., Hardy, R.J., Ferguson, R.I., Parsons, D.R., 2005. A framework for model verification and validation of CFD schemes in natural open channel flows. In: Bates, P.D., Lane, S.N., Ferguson, R.I. (Eds), Computational Fluid Dynamics: applications in environmental hydraulics. Wiley, New York, pp. 169-192.

Langendoen, E.J., Simon, A., 2008. Modeling the evolution of incised streams. II: Streambank erosion. J. Hydraul. Eng., 134(7), 905-915.

Langendoen, E.J., Mendoza, A., Abad, J.D., Tassi, P., Wang, D., Ata, R., El kadi Abderrezzak, K., Hervouet, J.-M., 2016. Improved numerical modelling of morphodynamics of rivers with steep banks. Adv. Water Resour. 93, 4-14.

Li, Y.-C., Chen, Y.M., Zhan, T.L.T., Ling, D.S., Cleall, P.J., 2010. An efficient approach for locating the critical slip surface in slope stability analyses using a real-coded genetic algorithm. Can. Geotech. J. 47, 806-820.

Malkinson, D., Wittenberg, L., 2007. Scaling the effects of riparian vegetation on cross-sectional characteristics of ephemeral mountain streams: a case study of Nahal Oren, Mt. Carmel, Israel. Catena 69, 103-110.

Meyer-Peter, E., Müller, R., 1948. Formulae for bed-load transport. 2nd IARH Congress. Stockholm: Sweden.

Midgley, T.L., Fox, G.A., Heeren, D.M., 2012. Evaluation of the bank stability and toe erosion model (BSTEM) for predicting lateral retreat on composite streambanks. Geomorphology 145–146, 107-114.

Minnesota Department of Transportation (MnDOT), 2015. Pavement design [technical report]. Office of materials and road research, Minnesota, United States.

Mitsch, W.J., Gosselink, J.G., 2010. Wetlands, 3rd Edition. Wiley, New York.

Murray, A. B., Paola, C., 2003. Modelling the effect of vegetation on channel pattern in bedload rivers. Earth Surf. Proc. Land., 28, 131-143.

Naval Facilities Engineering Command (NAVFAC), 1986. Design manual version 7.2 - Foundations and earth structures [technical report no. SN 0525-LP-300-7071]. Alexandria, Virginia.

Needelman, M., 2013. Évaluation du rôle des milieux humides dans l'espace de liberté par l'étude de la connectivité nappe-rivière [Master's thesis]. Université du Québec à Montréal, Montréal, Canada.

Parker, G., Shimizu, Z., Wilkerson, G.V., Eke, E.C., Abad, J.D., Lauer, J.W., Paola, C., Dietrich, W.E., Voller, V.R., 2011. A new framework for modeling the migration of meandering rivers. Earth Surf. Proc. Land. 36, 70-86.

Perucca, E., Camporeale, C., Ridolfi, L., 2007. Significance of the riparian vegetation dynamics on meandering river morphodynamics. Water Resour. Res. 43, W03430.

Pittaluga, M., Seminara, G., 2011. Nonlinearity and unsteadiness in river meandering: a review of progress in theory and modelling. Earth Surf. Proc. Land. 36, 20-38.

Pollen, N., 2007. Temporal and spatial variability in root reinforcement of streambanks: accounting for soil shear strength and moisture. Catena 69, 197-205.

Pollen-Bankhead, N., Simon, A., 2010. Hydrologic and hydraulic effects of riparian root networks on streambank stability: is mechanical root-reinforcement the whole story? Geomorphology 116, 353-362.

Posner, A.J., Duan, J.G., 2012. Simulating river meandering processes using stochastic bank erosion coefficient. Geomorphology 163–164, 26-36.

R Core Team, 2013. R: A language and environment for statistical computing. R Foundation for Statistical Computing, Vienna, Austria.

Rameshwaran, P., Naden, P., Wilson, C.A.M.E., Malki, R., Shukla, D.R., Shiono, K., 2013. Inter-comparison and validation of computational fluid dynamics codes in two-stage meandering channel flows. Appl. Math. Model. 37(20-21), 8652-8672.

Rinaldi, M., Mengoni, B., Luppi, L., Darby, S.E., Mosselman, E., 2008. Numerical simulation of hydrodynamics and bank erosion in a river bend. Water Resour. Res. 44, W09428.

Roache, P.J., Ghia, K.N., White, F.M., 1986. Editorial policy statement on the control of numerical accuracy. J. Fluid Eng.-T. ASME 108, 2.

Rousseau, Y.Y., Biron, P.M., Van de Wiel, M.J., 2014a. Implementation of geotechnical and vegetation modules in Telemac to simulate the dynamics of vegetated alluvial floodplains. In: Bertrand, O., Coulet, C. (Eds.), 21st Telemac-Mascaret User Conference. Artelia Eau & Environnement, Echirolles, Grenoble, France, pp. 169-177.

Rousseau, Y.Y., Van de Wiel, M.J., Biron, P.M., 2014b. Integration of a geotechnical model within a morphodynamic model to investigate river meandering processes. In: Schleiss, A.J., de Cesare, G., Franca, M.J., Pfister, M. (Eds.), 7th International Conference in Fluvial Hydraulics - River Flow. CRC Press / Balkema, London, UK, pp. 1127-1133.

Rousseau, Y.Y., Biron, P.M., Van de Wiel, M.J., 2016. Sensitivity of simulated flow fields and bathymetries in meandering channels to the choice of a morphodynamic model. Earth Surf. Proc. Land. 41(9), 1169-1184.

Rüther, N., Olsen, N. R. B., 2007. Modelling free-forming meander evolution in a laboratory channel using three-dimensional computational fluid dynamics. Geomorphology, 89(3-4), 308-319.

Schwenk, J., Lanzoni, S., Foufoula-Georgiou, E., 2015. The life of a meander bend: Connecting shape and dynamics via analysis of a numerical model. J. Geophys. Res. - Earth Surf. 120, 690-710.

Shen, H.W., 1984. Examination of present knowledge of river meandering. In: Elliot, C.M. (Ed.), River Meandering - Proceedings of the Conference Rivers '83. American Society of Civil Engineers, New Orleans, New York, pp. 1008-1012.

Simon, A., Curini, A., Darby, S.E., Langendoen, E.J., 2000. Bank and near-bank processes in an incised channel. Geomorphology 35, 193-217.

Smagorinsky, J., 1963. General circulation experiments with the primitive equations. Monthly Weather Review 91, 99-164.

Swiss Standard SN 670 010b, 1999. Characteristic coefficients of soils [technical report]. Association of Swiss Road and Traffic Engineers.

Tal, M., Paola, C., 2010. Effects of vegetation on channel morphodynamics: results and insights from laboratory experiments. Earth Surf. Proc. Land. 35, 1014-1028.

Therneau, T., Atkinson, B., Ripley, B., 2015. rPart - Recursive partitioning for classification, regression and survival trees [computer software]. R package version 4.1-10.

Thomas, R.E., Pollen-Bankhead, N., 2010. Modeling root-reinforcement with a Fiber-Bundle Model and Monte Carlo simulation. Ecol Eng 36, 47-61.

Thorne, C.R., 1982. Processes and mechanisms of river bank erosion. In: Hey, R.D., Bathurst, J.C., Thorne, C.R., (Eds.), Gravel-bed rivers. Wiley, New York, 227-270.

Tubbs, C.H., 1977. Root-crown relations of young Sugar Maple and Yellow Birch [Research Note NC-225]. USDA Forest Service.

University of Western Ontario, 2006. Light Detection and Ranging (LIDAR) (Last Pulse) digitation elevation model [computer file].

Van de Wiel, M.J., Darby, S.E., 2004. Numerical modeling of bed topography and bank erosion along tree-lined meandering rivers. In: Bennett, S.J., Simon A. (Eds.), Riparian Vegetation and Fluvial Geomorphology. American Geophysical Union, Washington, DC, 267-282.

Van de Wiel, M.J., Darby, S.E., 2007. A new model to analyse the impact of woody riparian vegetation on the geotechnical stability of riverbanks. Earth Surf. Proc. Land. 32, 2185-2198.

Vidal, J.-P., Moisan, S., Faure, J.-B., Dartus, D., 2007. River model calibration, from guidelines to operational support tools. Environ. Model. Softw. 22, 1628-1640.

Villaret, C., 2010. SISYPHE 6.0 User manual (H-P73-2010-01219-FR) [technical report]. National hydraulic and environment laboratory. EDF R&D, Chatou, France.

Williams, R.D., Brasington, J., Hicks, D.M., 2016a. Numerical modelling of braided river morphodynamics: review and future challenges. Geography Compass, 10(3), 102-127.

Williams, R.D., Measures, R., Hicks, D.M., Brasington, J., 2016b. Assessment of a numerical model to reproduce event-scale erosion and deposition distributions in a braided river. Water Resour. Res., 52, 6621-6642.

Youden, W.J., 1950. Index of rating diagnostic tests. Cancer, 3, 32-35.

Zolezzi, G., Seminara, G., 2001. Downstream and upstream influence in river meandering. Part 1. General theory and application to overdeepening. J. Fluid Mech. 438, 183-211.

Zolezzi, G., Luchi, R., Tubino, M., 2012. Modeling morphodynamic processes in meandering rivers with spatial width variations. Rev. Geophys., 50, RG4005.

Simulating bank erosion over an extended natural sinuous river reach using a universal slope stability algorithm coupled with a morphodynamic model

Yannick Y. Rousseau [a,*], Marco J. Van de Wiel [b], Pascale M. Biron [a]

[a] *Department of Geography, Planning and Environment, Concordia University, Henry F. Hall Building, Room S-H 1263, 1455 de Maisonneuve Blvd. W., Montréal, Canada, H3G 1M8. E-mail addresses: yanrousseau@gmail.com and pascale.biron@concordia.ca.*

[b] *Centre for Agroecology, Water and Resilience, Coventry University, James Starley Building, Room B02B, Priory Street, Coventry, United Kingdom, CV1 5FB. E-mail address: marco.vandewiel@coventry.ac.uk.*

Highlights

- A framework is proposed to model river bank erosion in a physics-based manner.

- Simulating bank erosion in a river channel requires a detailed geotechnical module.

- A genetic algorithm allows rotational and translational failures, and long scales.

- Lateral retreat is simulated independently of mesh structure and channel type.

- Predicted river bank failures agree with observations made in an alluvial channel.